applied optics

High-precision THz-TDS via self-referenced transmission echo method

Jon Gorecki,[1,*] Nicholas Klokkou,[1] Lewis Piper,[2] Sakellaris Mailis,[3] Nikitas Papasimakis,[1] and Vasilis Apostolopoulos[2]

[1]Optoelectronics Research Centre, University of Southampton, Southampton SO17 1BJ, UK
[2]School of Physics and Astronomy, University of Southampton, Southampton SO17 1BJ, UK
[3]Skolkovo Institute of Science and Technology, Moscow 143026, Russia
*Corresponding author: J.Gorecki@soton.ac.uk

Received 20 February 2020; revised 27 April 2020; accepted 28 April 2020; posted 28 April 2020 (Doc. ID 391103); published 30 July 2020

Terahertz time-domain spectroscopy (TDS) is a powerful characterization technique which allows for the frequency-dependent complex refractive index of a sample to be determined. This is achieved by comparing the time-domain of a pulse transmitted through air to a pulse transmitted through a material sample; however, the requirement for an independent reference scan can introduce errors due to laser fluctuations, mechanical drift, and atmospheric absorption. In this paper, we present a method for determining complex refractive index without an air reference, in which the first pulse transmitted through the sample is compared against the "echo", where the internal reflections delay the transmission of the echo pulse. We present a benchmarking experiment in which the echo reference method is compared to the traditional air method, and show that the echo method is able to reduce variation in real refractive index.

https://doi.org/10.1364/AO.391103

1. INTRODUCTION

Terahertz time-domain spectroscopy (THz-TDS) is a powerful analytical technique for investigating a wide range of materials such as spectroscopy of biological samples [1–4], detection of concealed drugs and explosives [5–7], imaging of astronomical objects [8,9], and industrial quality control of semiconductor manufacturing [10,11]. THz-TDS is unlike many spectroscopy methods, as it allows for both the real and imaginary parts of the refractive index to be determined due to the ability to measure the electric field in the time-domain at the sub-picosecond resolution [12]. The THz-TDS method relies on taking a suitable reference scan by which the sample scans are normalized, which is normally achieved by measuring the THz pulse transmitted through air, placing a sample in the beam path, and measuring the THz pulse through the sample. If the THz pulse is not correctly referenced, or the spectrometer has drifted since the reference scan, this can lead to errors in the complex refractive index which could, for example, cause the misidentification of an explosive security sample or failure to detect changes in a temporally evolving biological system.

There are many practical issues to address when referencing a THz scan in order to obtain reliable material characterization. One major issue to highlight from the air referencing method is that a THz spectrometer may experience fluctuations in the laser power between taking an air measurement and a sample measurement. This effect is especially compounded when it is required to take repeat measurements of samples over a long time period, such as several hours, to investigate a temporally changing system. Furthermore, when taking an air reference measurement, the sample must be removed/added to the optical system, which may not be physically possible in some situations; for example, with a sample held in a sealed chamber or other enclosed space. When taking a measurement with an air reference, it is generally assumed the complex refractive index of the air is $1 + 0i$, i.e., the air has identical refractive index to that of a vacuum; however, in practical cases, there is often atmospheric moisture, which can cause absorption of the THz pulse. After the air reference is taken and the sample is placed in the spectrometer, the beam then passes through less water vapor, which can skew the values of imaginary refractive index and register in the system as an artificial gain in intensity.

A self-referencing method to measure the strength of absorption peaks has been demonstrated in which a Fourier transform is applied to the time-domain signal with an ever-increasing window size [13]. In this manner, the frequency resolution of the data increases with the window size, allowing the strength of sharp absorption lines to be resolved. The method requires no independent reference scan, but is effective at measuring

absorption peaks with a sharp spectral width, and is not applicable to obtaining the real refractive index. To overcome some of these referencing issues, internally reflected pulses transmitted through the sample can be utilized to increase the sensitivity of spectroscopy devices. Various groups have demonstrated techniques where the first transmitted pulse and the internally reflected "echo" pulses are both compared to the air reference, where the echo pulses contain extra information due to increased interaction with the sample [14–16]. To negate the requirement for an air reference, an oblique reflection mode can be used where a sample is mounted against a quartz slide and the first THz pulse reflects off the face of the quartz, while the second pulse enters the quartz and reflects off the sample. By comparison of the two pulses, the complex refractive index of the sample can be determined [17,18]. A similar technique has been presented in transmission mode to determine refractive index, where the first pulse transmitted through the sample is compared to the echo pulse, which is internally reflected in the sample before being transmitted. However, this technique was only shown to produce the refractive index averaged over the THz pulse bandwidth instead of the frequency-dependent values [19,20]. Echo-based self-referencing has been demonstrated in reflection mode with a sample placed on a polished mirror, in which internally reflected THz pluses are delayed in time as compared to the pulse reflected on the top surface [21]. By comparing the first reflected and echo pulse, the refractive index can be obtained without an independent air reference. Such methods may be tricky to achieve, as the reflected echo is highly dependent on the sample–mirror interface, requiring alignment of two flat surfaces without an air gap. Further, the use of THz reflection setups can impose additional alignment issues as compared to transmission modes.

Here, we address the issue of air referencing by presenting a method to determine the frequency-dependent complex refractive index of a sample without an air reference in transmission-mode THz-TDS as shown in Fig. 1(a). The method relies on internal reflections within the sample to produce echo pulses which can be normalized to each other, requiring only one measurement scan to obtain all necessary data. This method has a number of advantages over the traditional air referencing method, as both measurements can be taken in a single time-domain trace, which reduces the chances of drift in the spectrometer between measurements. Second, this method allows for the sample to be held securely in the optical setup at all times, which reduces chances of misalignment between repeated sample mountings and can allow for samples to be held in difficult-to-access places such as sealed chambers and thermal stages. Third, we propose that this "echo referencing" method reduces the need for dry inert gas, as the sample does not need to be added/removed from the setup and therefore the volume of atmospheric gas is not decreased by inserting the sample. Dry inert gasses are often pumped into the THz spectrometer in order to displace atmospheric moisture, but this requires the system to be fully enclosed, which can be costly and difficult to achieve. In this paper, we derive the relevant parameter extraction equations for referencing the echo pulse to the first transmitted pulse, and present a comparative study in which a lithium niobate sample is measured repeatedly over a 50 minute period and complex refractive index values are compared for the two extraction methods: for the first transmitted pulse referenced to an air measurement, and for the first echo pulse referenced to the first transmitted pulse. We show that for the real refractive index, the echo reference method is able to reduce deviation between repeat measurements at frequencies below 1 THz; however, at higher frequencies, the echo method becomes unstable and ultimately has a lower usable bandwidth than the air reference method, which extends up to 1.5 THz.

2. REFRACTIVE INDEX EXTRACTION THEORY

Figure 1(b) depicts the optical paths for the first transmitted pulse and the echo pulse within the crystal sample. By measuring the THz time-domain, the two pulses can be separated and individually converted into the frequency domain by a Fourier transform. The first pulse enters from air into the sample in a transformation which can be described by the Fresnel transmission function. The pulse then propagates through a length d of the sample, which can be described by a complex Beer Lambert exponential attenuation equation, and finally passes out of the sample into air, which can be described by a further Fresnel transmission equation. The total combination of these functions describes the transmitted wave termed X_1 as shown in Eq. (1):

$$X_1 = A \cdot T_{ab} \cdot P_d \cdot T_{ba}, \tag{1}$$

where A is the arbitrary power of the incoming pulse, T_{ab} is the complex Fresnel transmission coefficient passing from material a into b, and P_d is the Beer Lambert term $P_d = \exp(-i\tilde{n}\omega d/c)$, where d is the thickness of material, and c is the speed of light. The echo pulse termed X_2 is described by Eq. (2):

$$X_2 = A \cdot T_{ab} \cdot P_d \cdot R_{ba} \cdot P_d \cdot R_{ba} \cdot P_d \cdot T_{ba}, \tag{2}$$

where R_{ba} is the complex Fresnel reflection coefficient from inside material b and bounding material a, with the form $R_{ba} = (\tilde{n}_b - \tilde{n}_a)/(\tilde{n}_b + \tilde{n}_a)$. By dividing the two pulses, the arbitrary power of the emitter A is removed, along with the transmission coefficients, leaving the complex transfer function termed H:

$$H = P_d^2 \cdot R_{ba}^2 = |Y(\omega)| \cdot e^{i\phi(\omega)}. \tag{3}$$

This transfer function H can be equated to the experimental data for the complex Fourier transform presented in unwrapped polar coordinates as $|Y(\omega)| \cdot e^{i\phi(\omega)}$, where $|Y(\omega)|$ is the magnitude and $\phi(\omega)$ is the unwrapped angle of the complex Fourier transform.

In the case in which $n \gg k$, then the Fresnel coefficients can be assumed to be real valued, which allows for the real and imaginary parts of the equations to be solved separately by rewriting the propagation constant in real and imaginary parts where $\tilde{n} = n + ik$. First, the real values of n can be calculated from

$$e^{-2in\omega d/c} = e^{i\phi(\omega)}, \tag{4}$$

and then plugged into

$$e^{2k\omega d/c} \cdot \left(\frac{n_a - n_b}{n_a + n_b}\right)^2 = |Y(\omega)| \tag{5}$$

to obtain the imaginary k components. For the case of an air-referenced sample, a similar extraction method is used

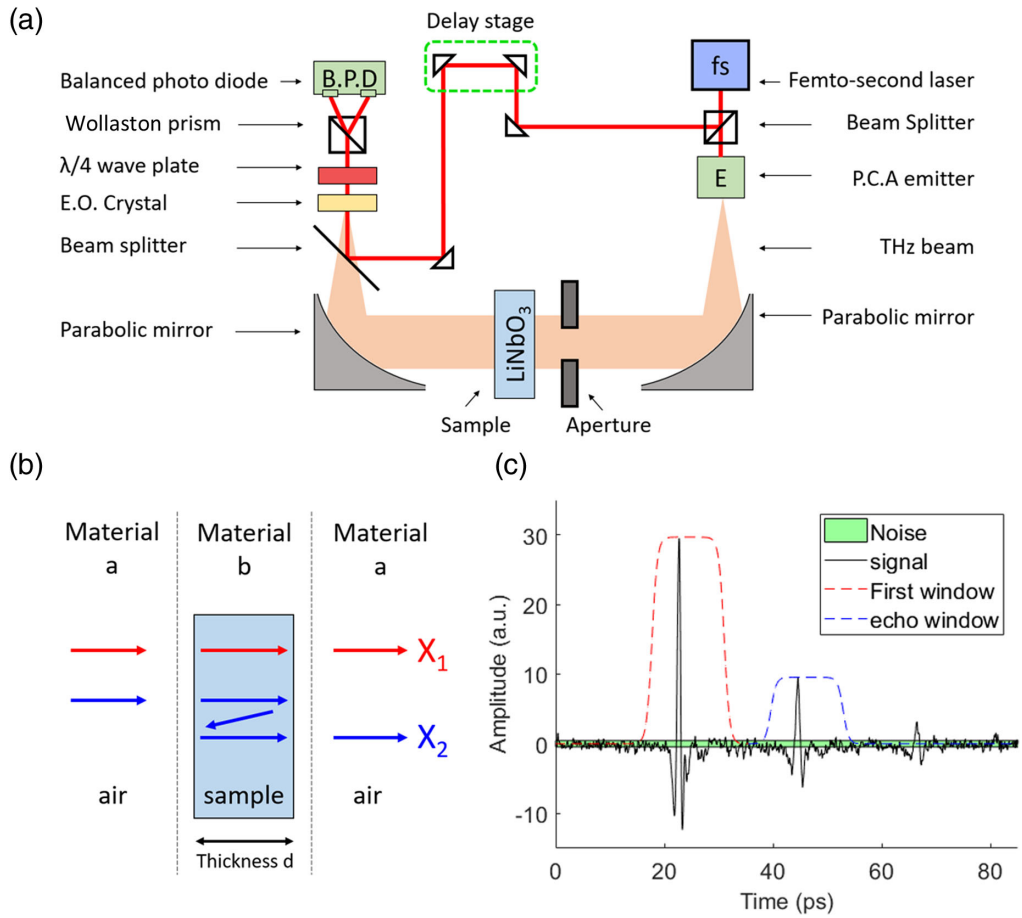

Fig. 1. (a) Schematic diagram of THz-TDS setup. The THz pulse is created by a photo-conductive antenna (P.C.A) which is collimated and transmitted through the $LiNbO_3$ sample. The pulse is detected via use of an electro-optic (E.O.) crystal and balanced photodiode. (b) Pulse propagation: Paths are shown for the first transmitted pulse (X_1) and the first internally reflected, or "echo" pulse (X_2) traveling from air, through a sample, and re-emerging to air. (c) Time-domain spectrum: The THz pulse passes through the $LiNbO_3$ sample, resulting in a peak around 20 ps. Due to internal reflections in the sample, subsequent echo-peaks can be seen, each with successively diminished intensities. Exponentially damped windows are applied to the first transmitted and first echo pulses. The noise of the detector (taking the standard deviation of the signal in the 30 ps period before the arrival of the first pulse) is highlighted by the green bar.

to calculate n and k as described in the literature [12]. The assumption of separable solutions for $n \gg k$ is valid in the case of lithium niobite, where the real part of the refractive index is over 100 times greater than the imaginary part. For the case where there is not such a large difference between n and k values, the real and complex solutions must be found simultaneously [12]. It should be noted that this method is not specific to use on the first transmitted and first echo pulse, and in fact any pair of subsequent echo pulses can be analyzed in this fashion without modification to the extraction equations presented here.

3. METHOD

A z-cut crystal of congruent lithium niobate is mounted on top of a metallic aperture of 10 mm diameter and placed in the beam path of a collimated THz source, as shown in Fig. 1(a). The sample thickness is measured with digital calipers to be 0.5 mm ($\pm$ 0.03 mm). The use of a collimated THz beam ensures normal incidence on the sample surface, which is required by the Fresnel equations we have used. The THz spectrometer is a commercially available Zomega spectrometer which detects THz radiation via femtosecond pulse interaction in a nonlinear crystal. A reference scan is first taken in the absence of the lithium niobate crystal through the metallic aperture; the lithium niobate is then mounted in the aperture and THz spectra are recorded with an averaging period of 2 min, recording a total of 24 spectra over a 50 min period. A fast-scan mechanism is employed in which the delay stage oscillates at 2 Hz, collecting multiple scans over a 2 min period. The use of the fast scan mechanism enables a large time-domain to be measured without significant increase in measurement time, although as the scan length increases the data resolution is correspondingly decreased. This effect is balanced, however, as in our case we obtain all data in a single trace instead of the usually obtained air trace and sample trace; therefore, we take one long measurement instead of two shorter measurements, and further do not need to account for time taken to add/remove the sample from the optics setup. All measurements are performed in an ambient air environment.

4. RESULTS

Figure 1(c) shows the time-domain of the THz radiation passing through the lithium niobate sample, where the first pulse (around 20 ps) corresponds to the pulse, which passes once through the sample, while the second pulse (around 45 ps) corresponds to the echo pulse, which is delayed in time due to the internal reflections within the sample. It can be seen that the echo pulse amplitude is attenuated in comparison to the first transmitted pulse due to the additional material interaction of the THz radiation with the sample due to the internal reflections. It can also be seen that there are additional echo pulses at 65 ps and 80 ps, but these are strongly attenuated and therefore we use only the first two peaks for the parameter extraction. The two pulses are separated from each other by multiplying the time-domain by an exponentially damped window, as shown by the dashed lines.

All pulses (measured through air or lithium niobate) are transformed with a window function. The window function is described by $W(t) = 1/(\exp((t - t0)/c) + 1)$, where c is 0.5 ps. An overlap between the first transmitted pulse and echo pulse always exists as the pulses extend infinitely in the time-domain. In the time-domain in Fig. 1(c), we highlight the standard deviation of the amplitude noise averaged over the 30 ps period before the arrival of the first pulse. From this figure it, can be seen that the signal of the first pulse descends into the noise level before the arrival of the echo pulse. The width of the windows is chosen to encompass fully the area in which the pulse signal is higher than the signal noise level. This process is not unimpeachable, but a full discussion of the windowing of time-domain pulses is far beyond the scope of this paper.

Figure 2(a) displays the amplitude of the frequency spectra obtained by Fourier transform for the pulse traveling through air, and the first pulse and echo pulse transmitted through lithium niobate. The transmission spectra reveal that the pulse through air has a usable bandwidth up to 3 THz, while lithium niobate has low transmission at frequencies above 1.5 THz for the first transmitted pulse, which is due to a phonon feature around 4 THz [22]. The echo pulse has a lower usable bandwidth than the first transmitted pulse, hitting the noise floor around 1 THz.

Once the Fourier transforms are performed, the magnitude of the echo pulse is divided by that of the first pulse to obtain $|Y(\omega)|$ while the unwrapped phase of the echo pulse is subtracted from that of the first pulse to obtain $\phi(\omega)$, and the complex refractive index is calculated. Figure 2(b) displays the real part of the refractive index of z-cut lithium niobate averaged for 24 measurements taken over a 50 min period, with the standard deviation shown as the shaded regions. The data is extracted with two different methods; in the first method, labeled "air reference," a reference measurement of THz propagation through air is taken before sample measurements and all subsequent lithium niobate measurements are normalized to this single air reference. In the second method, labeled "Echo Reference," the data is extracted by referencing the echo pulse to the first transmitted pulse, as described in the theory section.

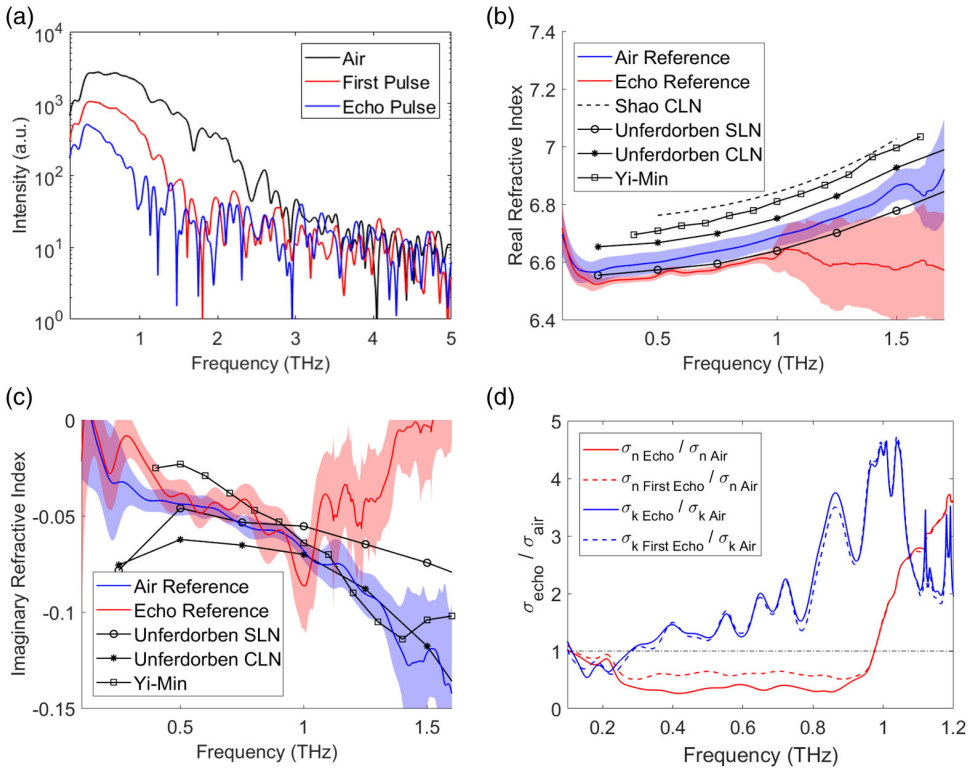

Fig. 2. (a) Frequency-domain spectra of pulse traveling through air and lithium niobate, and the first echo pulse. (b) and (c) Real and imaginary refractive index averaged for 24 measurements of lithium niobate over a 50 min period, where the error bars are given by the standard deviation of the repeat measurements. The blue datasets show the refractive index calculated by referencing to a measurement in air, while the red datasets use the echo referencing method. Previously reported values of refractive index are reproduced from the literature [23–25]. (d) Comparison of standard deviation from "air", "echo", and "first echo" methods showing ratio of echo methods to air method.

In the frequency range 0.1–1.0 THz, both methods result in similar values for real refractive index, where the echo method is on average 0.73% lower than for the air reference method. It can be seen from the graph that the air reference method is capable of providing trustworthy values up to 1.5 THz, while the echo pulse method suffers from large noise above 1 THz. However, in the region of 0.1 to 1 THz, it is clear that the echo pulse method has a much smaller standard deviation than the air reference method.

Overlaid to our experimental values of refractive index are those reported from Shao [23], Unferdorben [24], and Yi-Min [25]. There appears to be a relatively large variation in the reported values, which may be due to inherent differences in the crystal, measurement environments, or artificial differences—for example, from spectrometer alignment or extraction algorithms. The literature values reveal a large degree of variation, where the average range of literature values is 0.20 in this frequency region. Nevertheless, the value of refractive index we measure here are in general accordance with those reported from the literature. To compare all datasets, we look at the frequency range 0.5–1.0 THz, as this is the only range in which all datasets overlap. In this range, we find that the air reference method results in a real refractive index on average 1.06% lower than the average value from the literature, while the echo reference method is on average 1.89% lower.

Figure 2(c) shows imaginary refractive index extracted by the air and echo reference methods for 24 repeat measurements of lithium niobate where mean values are plotted as solid lines, with standard deviation plotted as colored error bars. Both extraction methods provide values which are in general accordance with the reported literature [23–25].

Figure 2(d) presents a comparison of the variation between the two referencing methods. The standard deviations of n and k for the echo method are divided by the deviation calculated using the air reference method. The echo method reduces the standard deviation for the real part of the refractive index between 0.1 and 1.0 THz, where the average value of the ratio is 0.35 in the frequency range 0.25–0.90 THz. The imaginary part, however, suffers from greater variation compared to the air method at all frequencies. This behavior is generally characteristic of THz-TDS where the imaginary components have greater variation than the real components; laser power fluctuations create variation in the imaginary components while the real components are affected by the drift of the mechanical delay stage, which is generally negligible in comparison.

It should be noted that we take 24 measurements through lithium niobate as compared to only one measurement through air; therefore, to compare the standard deviations of the air and echo methods may give a skewed impression of the statistical benefits. To further compare the two methods, we have also extracted data by the echo method in which every measurement of an echo pulse in lithium niobate is referenced to the first measurement of the first transmitted pulse which was taken at the beginning of the 50 min period (we will refer to this as the "first echo" method). In this manner, there is now a single reference scan for the air method and the "first echo" method. By division of the standard deviation of the "first echo" method by the air method, we see that the "first echo" method still achieves a reduction in the standard deviation for the real refractive index, while the imaginary components are relatively unchanged.

The large increase in standard deviation of the echo method above 1 THz is likely related to the echo pulse hitting the noise floor at this frequency [as shown in Fig. 2(a)]. To investigate whether this effect is indeed sample specific, we propose measuring silicon samples which display a relatively flat refractive index across 0.1–4.0 THz and should allow for the echo technique to be extended far beyond 1.0 THz.

5. SAMPLE COMPATIBILITY

The technique presented here imposes certain restrictions on the samples which can be measured. The thickness and refractive index of the sample must be large enough to effectively separate the multiply reflected pulses within the material so that they can be handled independently in the time-domain. By assessing the time-domain trace, we impose an exponential window on the pulses, by which we ensure span a time length sufficiently long to encompass the points at which the pulse descends into the noise level of the detector. From this, we can calculate the minimum separation of the first and echo peak, which ensures that the windows do no overlap at a level above the upper limit of the signal noise. The separation of the two pulse maxima is determined to be 16.9 ps. In Fig. 3(a), we plot the sample thickness d against refractive index n and highlight the region which allows for the necessary temporal separation of the two pulses, revealing a large region of material compatibility for samples.

To investigate the restrictions placed on the real part of the refractive index, we look towards the mathematical definition of the echo pulse presented in Eq. (2) (ignoring the Beer–Lambert propagation terms). By assessing the Fresnel terms of this equation, we see that the echo pulse is described by two transmission functions $T_{ab} \times T_{ba}$ and a squared reflection term R_{ab}^2. By plotting these two functions against refractive index n in Fig. 3(b), it can be seen that initially when $n = 1$, the transmission term is 1 while the reflection term is 0, which when multiplied together (red line) results in an echo pulse power of 0. As the refractive index increases, the transmission term decreases while the reflection term increases, which results in an echo power which initially increases and then tapers off, reaching a maximum around $n = 5.8$. For example, a measurement sample of silicon with refractive index $n = 3.4$ would exhibit an echo pulse power only 15% lower than for lithium niobate based on the Fresnel terms, demonstrating the wide range of material compatibility to the echo method.

The damping of the pulse as it propagates through a material is determined by the Beer–Lambert term, which increases exponentially with the imaginary part of the refractive index. The strength of the first transmitted pulse and echo pulse can be increased by choosing a sample material with a low k value, such as Si or GaAs, which are both around 40 times smaller in comparison to lithium niobate (at 1 THz, $k_{\mathrm{LiNbO_3}} = 0.07$ while $k_{si} \sim k_{\mathrm{GaAs}} \sim 0.0012$) [26]. Furthermore, the comparative benefits over the air referencing method will be dependent on the spectrometer hardware, such as the reliability of the mechanical delay stage, fluctuations in the laser power, and atmospheric humidity.

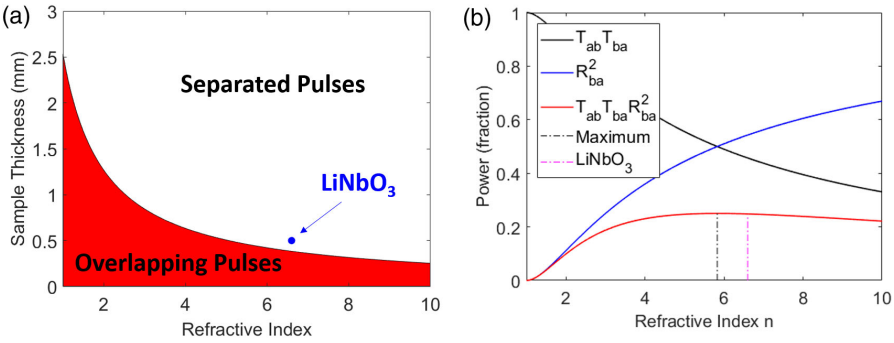

Fig. 3. (a) Theoretical power of echo pulse calculated by Fresnel coefficients reveals that the echo method is suitable for a broad range of refractive index values. (b) Diagram showing combination of sample thickness and refractive index which is capable of creating pulses separated in the time-domain. We plot the location of our 0.5 mm thickness lithium niobate sample, which reveals that even near the edge of the "separation" region, the method still functions adequately.

6. CONCLUSIONS

In conclusion, we have presented an "echo reference" method to determine complex refractive index from THz-TDS data in the absence of an air reference measurement. We present a benchmark test in which a test sample of lithium niobate is measured repeatedly over a 50 min period, and the data is extracted by both the echo reference and air reference methods. It is shown that for frequencies below 1 THz, the echo reference measurements achieve lower standard deviation in real refractive index values as compared to the air reference method, but the usable frequency bandwidth for the echo reference is lower than that of the air reference method. We argue the echo reference method has a number of advantages over a traditional air referencing method such as reduced effects of power drift, reduces the need for purging of the spectrometer chamber with inert gas, and allows the sample to be held securely in the optical setup without the need for removing the sample between measurements.

Funding. Engineering and Physical Sciences Research Council (EP/N509747/1).

Disclosures. The authors declare no conflicts of interest.

REFERENCES

1. A. Markelz, A. Roitberg, and E. Heilweil, "Pulsed terahertz spectroscopy of DNA, bovine serum albumin and collagen between 0.1 and 2.0 THz," Chem. Phys. Lett. **320**, 42–48 (2000).
2. S. Ebbinghaus, S. J. Kim, M. Heyden, X. Yu, U. Heugen, M. Gruebele, D. M. Leitner, and M. Havenith, "An extended dynamical hydration shell around proteins," Proc. Natl. Acad. Sci. USA **104**, 20749–20752 (2007).
3. M. Walther, B. Fischer, M. Schall, H. Helm, and P. Jepsen, "Far-infrared vibrational spectra of all-trans, 9-cis and 13-cis retinal measured by THz time-domain spectroscopy," Chem. Phys. Lett. **332**, 389–395 (2000).
4. R. M. Woodward, V. P. Wallace, R. J. Pye, B. E. Cole, D. D. Arnone, E. H. Linfield, and M. Pepper, "Terahertz pulse imaging of *ex vivo* basal cell carcinoma," J. Invest. Dermatol. **120**, 72–78 (2003).
5. J. F. Federici, B. Schulkin, F. Huang, D. Gary, R. Barat, F. Oliveira, and D. Zimdars, "THz imaging and sensing for security applications—explosives, weapons and drugs," Semicond. Sci. Technol. **20**, S266–S280 (2005).
6. R. Appleby and H. B. Wallace, "Standoff detection of weapons and contraband in the 100 GHz to 1 THz region," IEEE Trans. Antennas Propag. **55**, 2944–2956 (2007).
7. J. Chen, Y. Chen, H. Zhao, G. J. Bastiaans, and X.-C. Zhang, "Absorption coefficients of selected explosives and related compounds in the range of 0.1–2.8 THz," Opt. Express **15**, 12060–12067 (2007).
8. J. Wei, D. Olaya, B. S. Karasik, S. V. Pereverzev, A. V. Sergeev, and M. E. Gershenson, "Ultrasensitive hot-electron nanobolometers for terahertz astrophysics," Nat. Nanotechnol. **3**, 496–500 (2008).
9. M. Negrello, R. Hopwood, G. D. Zotti, A. Cooray, A. Verma, J. Bock, D. T. Frayer, M. A. Gurwell, A. Omont, R. Neri, H. Dannerbauer, L. L. Leeuw, E. Barton, J. Cooke, S. Kim, E. da Cunha, G. Rodighiero, P. Cox, D. G. Bonfield, M. J. Jarvis, S. Serjeant, R. J. Ivison, S. Dye, I. Aretxaga, D. H. Hughes, E. Ibar, F. Bertoldi, I. Valtchanov, S. Eales, L. Dunne, S. P. Driver, R. Auld, S. Buttiglione, A. Cava, C. A. Grady, D. L. Clements, A. Dariush, J. Fritz, D. Hill, J. B. Hornbeck, L. Kelvin, G. Lagache, M. Lopez-Caniego, J. Gonzalez-Nuevo, S. Maddox, E. Pascale, M. Pohlen, E. E. Rigby, A. Robotham, C. Simpson, D. J. B. Smith, P. Temi, M. A. Thompson, B. E. Woodgate, D. G. York, J. E. Aguirre, A. Beelen, A. Blain, A. J. Baker, M. Birkinshaw, R. Blundell, C. M. Bradford, D. Burgarella, L. Danese, J. S. Dunlop, S. Fleuren, J. Glenn, A. I. Harris, J. Kamenetzky, R. E. Lupu, R. J. Maddalena, B. F. Madore, P. R. Maloney, H. Matsuhara, M. J. Michaowski, E. J. Murphy, B. J. Naylor, H. Nguyen, C. Popescu, S. Rawlings, D. Rigopoulou, D. Scott, K. S. Scott, M. Seibert, I. Smail, R. J. Tuffs, J. D. Vieira, P. P. van der Werf, and J. Zmuidzinas, "The detection of a population of submillimeter-bright, strongly lensed galaxies," Science **330**, 800–804 (2010).
10. N. Nagai, M. Sumitomo, M. Imaizumi, and R. Fukasawa, "Characterization of electron- or proton-irradiated Si space solar cells by THz spectroscopy," Semicond. Sci. Technol. **21**, 201–209 (2006).
11. K. Ahi, S. Shahbazmohamadi, and N. Asadizanjani, "Quality control and authentication of packaged integrated circuits using enhanced-spatial-resolution terahertz time-domain spectroscopy and imaging," Opt. Lasers Eng. **104**, 274–284 (2018).
12. P. Jepsen, D. Cooke, and M. Koch, "Terahertz spectroscopy and imaging—modern techniques and applications," Laser Photon. Rev. **5**, 124–166 (2011).
13. A. Redo-Sanchez and X.-C. Zhang, "Self-referenced method for terahertz wave time-domain spectroscopy," Opt. Lett. **36**, 3308–3310 (2011).
14. P. R. Whelan, K. Iwaszczuk, R. Wang, S. Hofmann, P. Bøggild, and P. U. Jepsen, "Robust mapping of electrical properties of graphene from terahertz time-domain spectroscopy with timing jitter correction," Opt. Express **25**, 2725–2732 (2017).
15. J. Choi, W. S. Kwon, K.-S. Kim, and S. Kim, "Nondestructive material characterization in the terahertz band by selective extraction of sample-induced echo signals," J. Nondestruct. Eval. **34**, 269 (2014).

16. L. Duvillaret, F. Garet, and J.-L. Coutaz, "Highly precise determination of optical constants and sample thickness in terahertz time-domain spectroscopy," Appl. Opt. **38**, 409–415 (1999).
17. W. Lai, H. Cao, J. Yang, G. Deng, Z. Yin, Q. Zhang, B. Pelaz, and P. Del Pino, "Antireflection self-reference method based on ultrathin metallic nanofilms for improving terahertz reflection spectroscopy," Opt. Express **26**, 19470–19478 (2018).
18. S. Huang, P. C. Ashworth, K. W. Kan, Y. Chen, V. P. Wallace, Y. Ting Zhang, and E. Pickwell-MacPherson, "Improved sample characterization in terahertz reflection imaging and spectroscopy," Opt. Express **17**, 3848–3854 (2009).
19. F. Sanjuan, A. Bockelt, and B. Vidal, "Determination of refractive index and thickness of a multilayer structure with a single terahertz time domain spectroscopy measurement," Appl. Opt. **53**, 4910–4913 (2014).
20. F. Sanjuan and B. Vidal, "Refractive index calculation from echo interference in pulsed terahertz spectroscopy," Electron. Lett. **50**, 308–309 (2014).
21. F. Vandrevala and E. Einarsson, "Decoupling substrate thickness and refractive index measurement in THz time-domain spectroscopy," Opt. Express **26**, 1697–1702 (2018).
22. M. Dutta, C. Ellis, X. G. Peralta, A. Bhalla, and R. Guo, "Terahertz electrical and optical properties of $LiNbO_3$ single crystal thin films," Proc. SPIE **9586**, 958608 (2015).
23. G. Hao Shao, S. Jun Ge, Y. Chao Shi, W. Hu, and Y. Qing Lu, "Extended Cauchy equations of congruent LiNbO_3 in the terahertz band and their applications," Opt. Mater. Express **6**, 3766–3775 (2016).
24. M. Unferdorben, Z. Szaller, I. Hajdara, J. Hebling, and L. Pálfalvi, "Measurement of refractive index and absorption coefficient of congruent and stoichiometric lithium niobate in the terahertz range," J. Infrared Millim. Terahertz Waves **36**, 1203–1209 (2015).
25. S. Yi-Min, M. Zong-Liang, H. Bi-Hui, L. Guo-Qing, and W. Li, "Giant birefringence of lithium niobate crystals in the terahertz region," Chin. Phys. Lett. **24**, 414–417 (2007).
26. D. Grischkowsky, S. Keiding, M. van Exter, and C. Fattinger, "Far-infrared time-domain spectroscopy with terahertz beams of dielectrics and semiconductors," J. Opt. Soc. Am. B **7**, 2006–2015 (1990).